Synthesis, characterization and catalytic performance of samarium sesquioxide supported cobalt catalyst for methane dry reforming to syngas

Bamidele V. Ayodele,
Faculty of Chemical & Natural Resources Engineering, Universiti Malaysia Pahang,
Lebuhraya Tun Razak, 26300 Gambang Kuantan, Pahang Malaysia
bamidele.ayodele@uniben.edu

M. Anwar Hossain
Faculty of Chemical & Natural Resources Engineering, Universiti Malaysia Pahang,
Lebuhraya Tun Razak, 26300 Gambang Kuantan, Pahang Malaysia

Mohd Nasir Nor Shahirah
Faculty of Chemical & Natural Resources Engineering, Universiti Malaysia Pahang,
Lebuhraya Tun Razak, 26300 Gambang Kuantan, Pahang Malaysia

Maksudur R. Khan,
Faculty of Chemical & Natural Resources Engineering, Universiti Malaysia Pahang,
Lebuhraya Tun Razak, 26300 Gambang Kuantan, Pahang Malaysia

Chin Kui Cheng
Faculty of Chemical & Natural Resources Engineering, Universiti Malaysia Pahang,
Lebuhraya Tun Razak, 26300 Gambang Kuantan, Pahang Malaysia
E-mail: chinkui@ump.edu.my

Abstract- This study focuses on the synthesis, characterization and performance of $20wt\%Co/80wt\%Sm_2O_3$ catalyst in methane dry reforming for the production of syngas. The $20wt\%Co/80wt\%Sm_2O_3$ catalyst was synthesized via wet-impregnation method and characterized by TGA, FTIR, XRD, FESEM, EDX, N_2 physisorption and H_2-TPR. The performance of the catalyst in the methane dry reforming reaction was studied in a stainless steel fixed-bed continuous flow reactor at feed ($CH_4:CO_2$) ratio of 1.0, temperature ranged 923-1023K and GHSV of 30000 h^{-1}. The $20wt\%Co/80wt\%Sm_2O_3$ catalyst showed promising catalytic performance evident from the highest CH_4 and CO_2 conversion of $\sim$71% and $\sim$72% as well as the highest H_2 and CO yield of $\sim$62% and $\sim$73%, respectively. Moreover, the methane dry reforming over the $20wt\%Co/80wt\%Sm_2O_3$ catalyst produces H_2: CO ratio close to unity, hence suitable for use as a chemical intermediate for synthesis of oxygenated fuels. The characterization of the used $20wt\%Co/80wt\%Sm_2O_3$ catalyst used after 4 h of time-on-stream confirmed the presence of amorphous carbon which can easily be gasified.

Keywords: Methane dry reforming; Cobalt: Samarium sequioxide; Syngas.

1. INTRODUCTION

Synthesis gas (syngas), a mixture of carbon monoxide and hydrogen can be produced from catalytic reforming of methane [1]. Amongst the several catalytic reforming processes employed for the production of syngas, methane dry reforming is more beneficial in terms of energy production and mitigation of greenhouse effects. Theoretically, syngas ratio of unity is produced from methane dry reforming, making it suitable as a chemical building blocks for the synthesis of oxygenated fuels means of Fitscher-Tropsch Synthesis (FTS) [2,3]. Besides, the two main contributors to greenhouse gases are utilized for the reforming process, thereby mitigating the greenhouse effects on the environment [4,5]. Furthermore, the highly endothermic nature of the methane dry reforming reaction makes it suitable to be used in chemical energy transmission and storage system [6].

The main constraint to the methane dry reforming process is catalyst deactivation through coking and sintering [7,8]. The formation and deposition of coke on the catalyst's surface usually occur through side reactions such as methane cracking and reverse Boudouard [9]. The formation and depositions of coke via methane cracking is favoured at temperature > 973 K and low pressure while that of reverse Boudouard is favoured at temperature < 973 K and high pressure [10]. Moreover, the high temperature requirement for the methane dry reforming process as well as the action of the reverse water gas shift reaction makes the methane dry reforming catalyst susceptible to sintering [11].

In order to overcome the constraints in methane dry reforming, researchers have exploited the use of supported metal catalysts such as Co, Ni, Ru, Rh, Pd and Pt. Excellent review by Pakhare [12] showed that supported noble metals catalyst (Ru, Rh, Pd and Pt) exhibited good activity with less carbon deposition. However, they are expensive and not readily available. Nickel-based catalysts would have been a better alternative for the methane dry reforming process due to high activity but are easily prone to cooking and sintering [13]. Co-metals has a great potential to be used as catalysts for methane dry reforming due to its good activity, stability, non-pricey and availability [14–16].

The performance of non-noble metal-base catalysts such as Co can be enhanced through the use of suitable supports. The synthesis of the Co-metal on a suitable support will provide a beneficial synergy leading to the controlling of carbon formation[16]. Reports have shown that rare earth oxides based supports such as CeO_2 and La_2O_3 have high oxygen retention capacity [17]. The use of these supports enhances the formation of surface oxygen from dissociative adsorption of CO_2 which can be used to neutralise the carbon formed on the surface of the active metals. This study focuses on the synthesis, characterization, catalytic performance of Sm_2O_3 supported Co catalyst. The best of the author's knowledge, Co/ Sm_2O_3 catalyst has not been investigated for syngas production via methane dry reforming.

2. EXPERIMENTAL

2.1. Catalyst Synthesis and pretreatment

Prior to the synthesis of the catalyst, the Sm_2O_3 support was prepared by thermal decomposition of $Sm(NO_3)_3.6H_2O$ (99.99% purity, Sigma-Aldrich) at 873 K for 2 h according to the method described by Mohammadinasab et al. [18]. To obtain Co/Sm_2O_3 catalyst, the as-prepared Sm_2O_3 support was impregnated with aqueous solution of $Co(NO_3)_2.6H_2O$ (99.99% purity, Sigma-Aldrich) equivalent to 20wt% Co loading. The slurry after the impregnation was continuously stirred for 3 h to allow for aging of the Co precursor and thereafter dried 393 K for 24 h. The dried Co/Sm_2O_3 was calcined at 873 K for 6 h. Prior to the activity test, the calcined catalyst was reduced *in situ* in 50 ml min^{-1} of 20% H_2 in N_2 carrier gas for 1 h at 873 K.

2.2. Catalyst Characterization

The freshly prepared as well as the calcined 20wt%Co/80wt%Sm_2O_3 catalyst were characterized for physicochemical properties using several instruments techniques. The thermal stability of the uncalcined catalyst was determined by thermogravimetric analysis (TGA) (Thermal analyser instrument Q-500 series) under N_2 flow at heating rate of 10 K min^{-1} and atmospheric pressure. The nature of the chemical bonds in the calcined 20wt%Co/80wt%Sm_2O_3 catalyst was determined by FTIR (Perkin Elmer Spectrum 100). The spectra were collected at a resolution of 8 cm^{-1} using attenuated total reflectance (ATR) within the range of 4000-400 cm^{-1} and analysed using Ominic software. The phase identification and the crystallinity of the catalyst were measured by X-ray power diffraction analysis. The recording of the XRD diffractograms was done using a RIGAKU miniflex II X-ray diffractometer capable of measuring powdered diffraction pattern from 3 to 145° in 2θ scanning range. The X-ray source is Cu Kα with wavelength (λ) of 0.154 nm radiation. The XRD is equipped with the latest version of PDXL, RIGAKU full function powder-diffraction analysis software. The textural properties of the calcined 20wt%Co/80wt%Sm_2O_3 catalyst were determined using N_2-sorptiometry. Prior to the measurements, the as-prepared catalyst

sample was degassed at 523 K. The information about the surface morphology of the catalysts and the elemental chemical compositions were determined using JEOL field emission scanning electron microscopy (FESEM) equipped with energy-dispersive X-ray spectroscopy (EDX). The adsorption and desorption isotherm were obtained by measuring the amount of gas adsorbed and removed across relative pressure range 0.1-1.0 and reduced pressure using liquid N_2 at 77 K. The specific surface area and the pore volume of the catalyst sample were obtained from the adsorption-desorption isotherm using Brunauer-Emmett-Teller (BET) and Berreth-Joyner-Halenda (BJH) methods [19,20]. The reducibility of the catalyst was measured by H_2-temperature programmed reduction (H_2-TPR) using Thermo-Scientific TPDRO 1100 apparatus equipped with TCD detector. Approximately 60 mg of the catalyst sample was initially pre-treated in a flow of 20 ml min^{-1} N_2 at heating rate of 10 K min^{-1} up to 393 K at holding period of 30 min. Subsequently, the pre-treated catalyst sample was reduced with 20 ml min^{-1} of 5% H_2 in N_2 carrier gas at heating rate of 10 K min^{-1} up to 1173 K with holding period of 60 min before cooling to room temperature.

2.3. Catalytic performance evaluation

The performance of the 20wt%Co/80wt%Sm_2O_3 catalyst was evaluated in a continuous, top-down flow tubular stainless steel reactor of a fixed-bed configuration (internal diameter: 10 mm and height: 35 cm) as depicted in Figure 1. The methane dry reforming was performed using catalyst weighing 200 mg supported using quartz wool. The reactor system was equipped with Type-K thermocouple and PID temperature controller. The catalyst's performance was evaluated at 923 to 1023 K, with CH_4:CO_2 feed ratios between 0.1 and 1, at atmospheric pressure and total flow of 100 ml/min. The flow rate of the inlet gases (CH_4, CO_2 and N_2) were controlled by digital mass flow controllers. The gas hourly space velocity (GHSV) for the reaction was maintained at 30000 h^{-1} STP. Prior to the reaction, the catalyst was reduced in-situ in a flow of 50 ml/min H_2/N_2 (1:5) at 973 K for 1 h employing a ramping rate of 10 K min^{-1}. The reaction was performed at time-on-stream (TOS) of 4 h. The composition of exit gas was determined using gas chromatography instrument (GC-Agilent 6890 N series) equipped with TCD. Two packed columns were used, viz. Supelco Molecular Sieve 13x (10 ft × 1/8 in OD × 2mm ID, 60/80 mesh, Stainless Steel) and Agilent Hayesep DB (30 ft × 1/8 in OD × 2 mm ID, 100/120 mesh, Stainless Steel). Helium gas was used as the carrier with flowrate of 20 ml min^{-1} and operating column temperature of 393 K. The reported CH_4 and CO_2 conversions, as well as H_2 and CO yield represents an average of four analysis of the gaseous products at 1 h interval for 4 h TOS. The reaction metrics for the evaluation of the catalytic performance are represented in Equations (1) – (4):

$$CH_4 \text{ conversion (\%)} = \frac{F_{CH_{4in}} - F_{CH_{4out}}}{F_{CH_{4in}}} \times 100 \tag{1}$$

$$CO_2 \text{ conversion (\%)} = \frac{F_{CO_{2in}} - F_{CO_{2out}}}{F_{CO_{2in}}} \times 100 \tag{2}$$

$$H_2 \text{ yield} = \frac{F_{H_{2out}}}{2 \times F_{CH_{4in}}} \times 100 \tag{3}$$

$$CO \text{ yield} = \frac{F_{CO_{out}}}{F_{CH_{4in}} + F_{CO_{2in}}} \times 100 \tag{4}$$

where $F_{CO_{2in}}$, $F_{CH_{4in,}}$, $F_{CO_{2out}}$, $F_{CH_{4out}}$ are the inlet and outlet molar flow rate of CO_2 and CH_4, respectively, and $F_{H_{2out}}$ is the

outlet molar flow rate of H_2.

3. RESULTS AND DISCUSSION

3.1 Catalyst characterization

The thermogravimetric analysis of the fresh 20wt%Co/80wt%Sm_2O_3 catalyst showing the TG and the DTG curves are depicted in Figure 2. The TG and the DTG curves represent different staged of the decomposition of the catalyst precursor which can be categorized into four stages represented by peaks I-IV. Peak I can be attributed to the sequential loss of physical water as well as sequential dehydration of $Co(NO_3)_2 . 6H_2O$ at temperature ranged 270-440 K. Peaks II, III, and IV at temperature ranged 440-850 K can be attributed to the sequential decomposition of the cobalt nitrate species. The disappearance of the DTG curve beyond 850 K is evidence that the catalyst is present in its pure state. This observation is corroborated with the FTIR analysis shown in Figure 3 (which shows an absence of nitrate functional group). This is also consistent with the findings of Ehrhardt et al. [21] for thermal decomposition of nitrate-compounds.
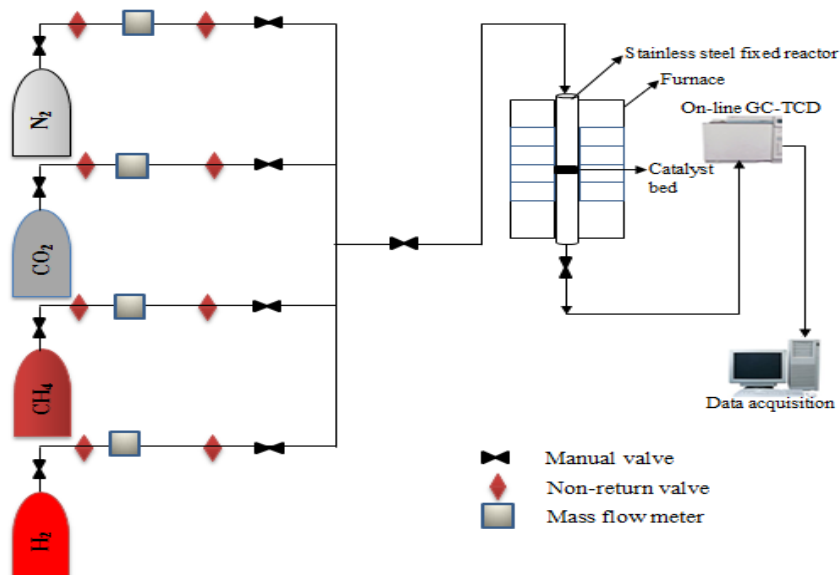
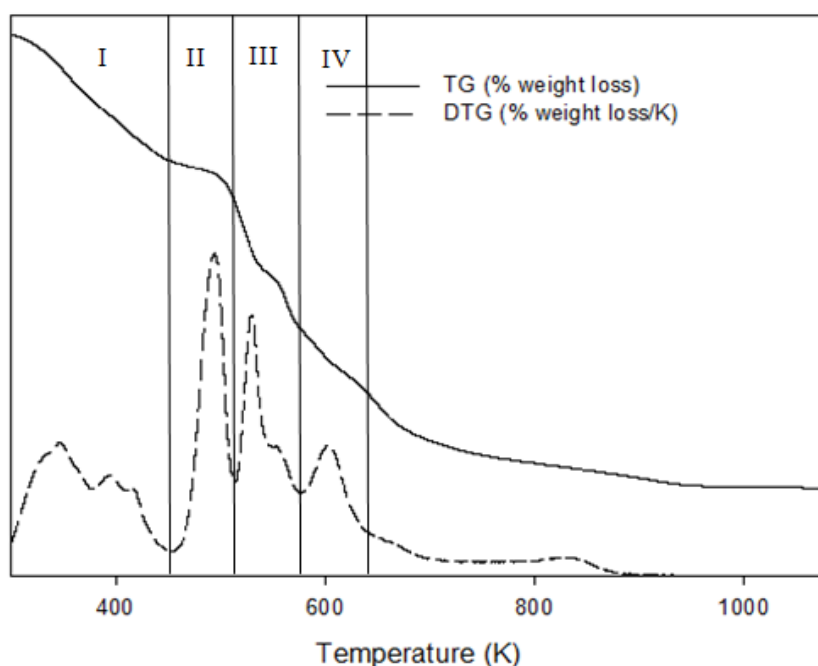Figure 1: Schematic representation of the experimental set up for the syngas production over 20wt%Co/80wt%Sm$_2$O$_3$ catalyst.

Figure 2: TG and DTG profiles for temperature programmed calcination of fresh 20wt%Co/80wt%Sm$_2$O$_3$

Figure 3 show the FTIR spectra of the freshly-calcined 20wt%Co/80wt%Sm$_2$O$_3$ in comparison with the Sm(NO$_3$)$_3$.6H$_2$O. The spectra for the 20wt%Co/80wt%Sm$_2$O$_3$ catalyst shows a broad band centred around 578, 673, and 1411 cm^{-1}, symptomatic of Sm-O stretching vibration, Co-O stretching vibration, and C=O bond which can be attributed to the presence of Sm$_2$O$_3$, Co$_3$O$_4$ and dissolved atmospheric CO$_2$. The N-O bond in the precursors signifies the presence of nitrates prior to decomposition. After decomposition of the precursors, both the OH and N-O bonds (3256 and 3185 cm^{-1}) disappeared, which is an evidence of the pure state of 20wt%Co/8-wt%Sm$_2$O$_3$ catalyst as can be seen from the spectra. The presence of the catalyst in its pure state is due to the removal of physical and hydrated water, as well as decomposition of the nitrate during the temperature-programmed calcination. The as-prepared catalyst which is made of Sm$_2$O$_3$ and Co$_3$O$_4$ is confirmed by the Sm-O and Co-O stretching vibration of the FTIR spectra, which is also corroborated by the XRD pattern shown in Figure 4.
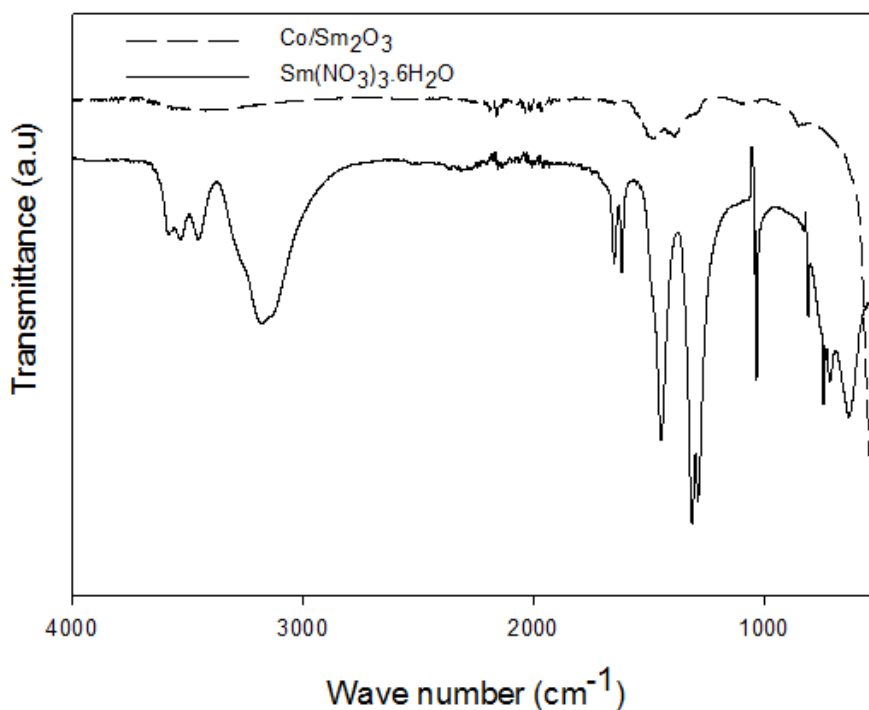
Figure 3: FTIR spectra of the fresh 20wt%Co/80wt%Sm$_2$O$_3$ catalyst and Sm(NO$_3$)$_3$.6H$_2$O
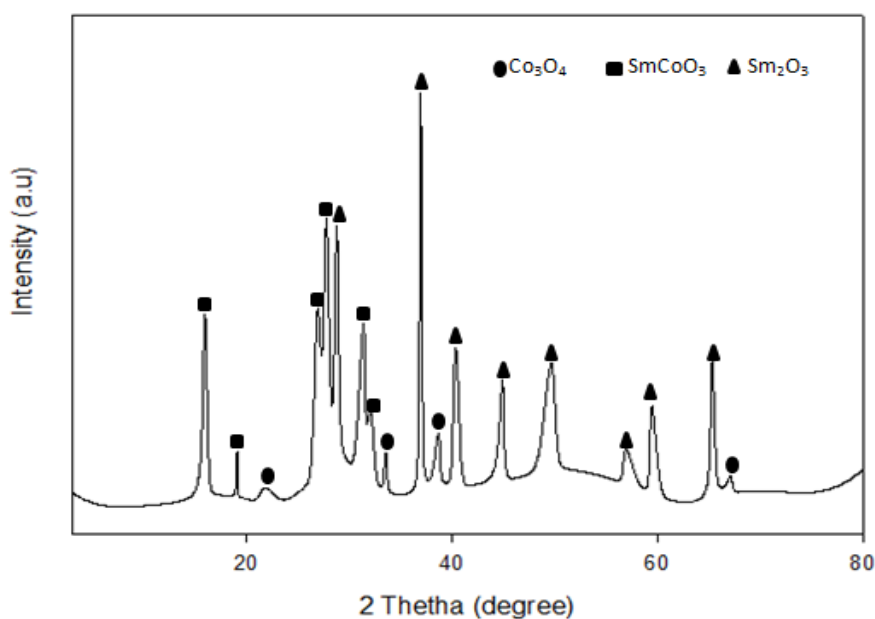

Figure 4: The XRD pattern of the fresh 20wt%Co/80wt%Sm$_2$O$_3$ catalyst

Figure 4 shows the XRD pattern of the freshly calcined 20wt%Co/80wt%Sm$_2$O$_3$. Significantly, three crystalline phases namely Co$_3$O$_4$, SmCoO$_3$ and Sm$_2$O$_3$ can be identified from the XRD pattern as summarized in Table 2. The spinel Co$_3$O$_4$ crystals at 21.7° (1 3 1), 33.53° (2 1 1), 38.67° (2 2 2) and 67.14 (1 3 1) can be attributed to the body-centred cubic and face-centred cubic phases. In addition, the Sm$_2$O$_3$ crystals identified at 28.74° (1 0 1), 36.87° (1 1 1), 40.29° (2 0 1), 44.91° (4 0 0), 49.68° (3 3 1), 56.79° (1 1 2), 59.33° (5 1 1) and 65.33° (4 4 0) can be attributed to the body-centred cubic phase. Interestingly, SmCoO$_3$ perovskite can be identified at 15.87° (1 0 0), 19.02° (1 1 1), 26.89° (1 0 1), 27.73° (1 1 0), 31.36° (2 2 0) and 32.08° (2 0 0) representing mostly body-centred cubic and face-centred cubic phases. The formation of SmCoO$_3$ could be as a result of strong interaction between the Co$_3$O$_4$ and Sm$_2$O$_3$ during the calcination stage. Furthermore, the average crystallites sizes for Co$_3$O$_4$, Sm$_2$O$_3$ and SmCoO$_3$ were estimated from the Scherer's equation using full-width-half-maximum (FWHM) of the respective XRD peaks as 26.12, 19.84 and 21.21 nm respectively.
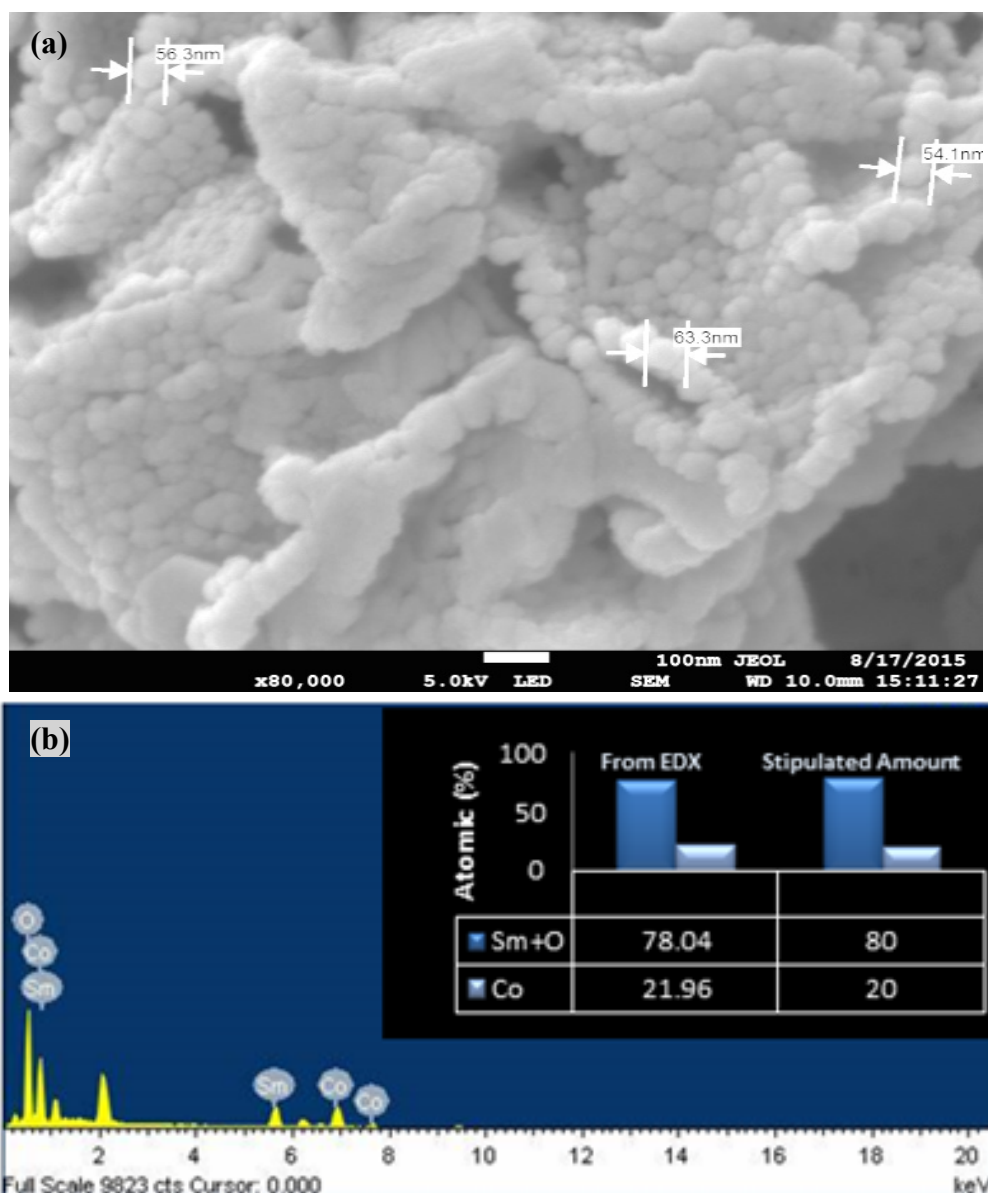
Figure 5: (a) FESEM image and (b) EDX micrograph showing the elemental composition of the catalyst and

The FESEM micrographs and EDX analysis showing the morphology and elemental composition of the freshly calcined 20wt%Co/80wt%Sm_2O_3 is depicted in Figure 5. It can be seen that the 20wt%Co/80wt%Sm_2O_3 catalyst exhibits small spherical-shaped particles with evidence of weak agglomeration. The particle diameters of the 20wt%Co/80wt%Sm_2O_3 measured at three different spots were recorded as 56.3, 54.1 and 63.3 nm. The EDX analysis for the elemental compositions of the as-prepared 20wt%Co/80wt%Sm_2O_3 is depicted in Figure 5 (a). It is noteworthy that all the components (Co, Sm and O) of the as-synthesized 20wt%Co/80wt%Sm_2O_3 catalysts can be identified from the EDX analysis. Interestingly, the composition of 21.96% and 78.04% obtained for Co and Sm_2O_3 is consistent with the stipulated amount used for the catalyst synthesis.

The BET specific surface area, as well as the BJH pore volume of the 20wt%Co/80wt%Sm_2O_3 catalyst and Sm_2O_3 support alone are shown in Figure 6. The adsorption-desorption isotherm exhibits a Type-IV curve with H2-type hysteresis according to IUPAC classification. The inflection points at P/P^o ranged 0.45-0.95 is an indication of the capillary condensation within uniform mesopores. The BET specific surface of 9.53 m^2/g obtained for the Sm_2O_3 support is smaller compared to the 23.05 m^2/g obtained for the 20wt%Co/80wt%Sm_2O_3 catalysts. This could be attributed to the well-dispersed Co particles on the support which invariably leads to higher BET specific surface area. Moreover, the higher values of the pore volume and the pore diameter obtained for the 20wt%Co/80wt%Sm_2O_3 catalyst compared to the Sm_2O_3 support is also evidence of the well

dispersed Co particles. This has created additional macropores as clearly visible in the FESEM images (refers to Figure 5), therefore an increase in textural properties.

The reducibility of the freshly calcined 20wt%Co/80wt%Sm$_2$O$_3$ represented by the H$_2$-TPR profile is depicted in Figure 7. Interestingly the TPR curves of the catalyst displayed two major reduction peaks cantered at 730 K and 865 K. These peaks are indication of different degree of Co-Sm$_2$O$_3$ interaction displayed by Co$_3$O$_4$, and SmCoO$_3$ species. The temperature reduction at 730 K could be attributed to the H$_2$-reduction of the Co$_3$O$_4$ phase to Co° and the second peak cantered at 865 K corresponds to the H$_2$-reduction of SmCoO$_3$ to Co° and Sm$_2$O$_3$ which is consistent with the XRD pattern of the used catalyst (initially reduced at 873K) (cf. Figure 11). The H$_2$-uptake for the reduction of the Co phases is estimated from the TPDRO 1100 as 3634.38 and 5085.60 µmol g^{-1}, respectively.
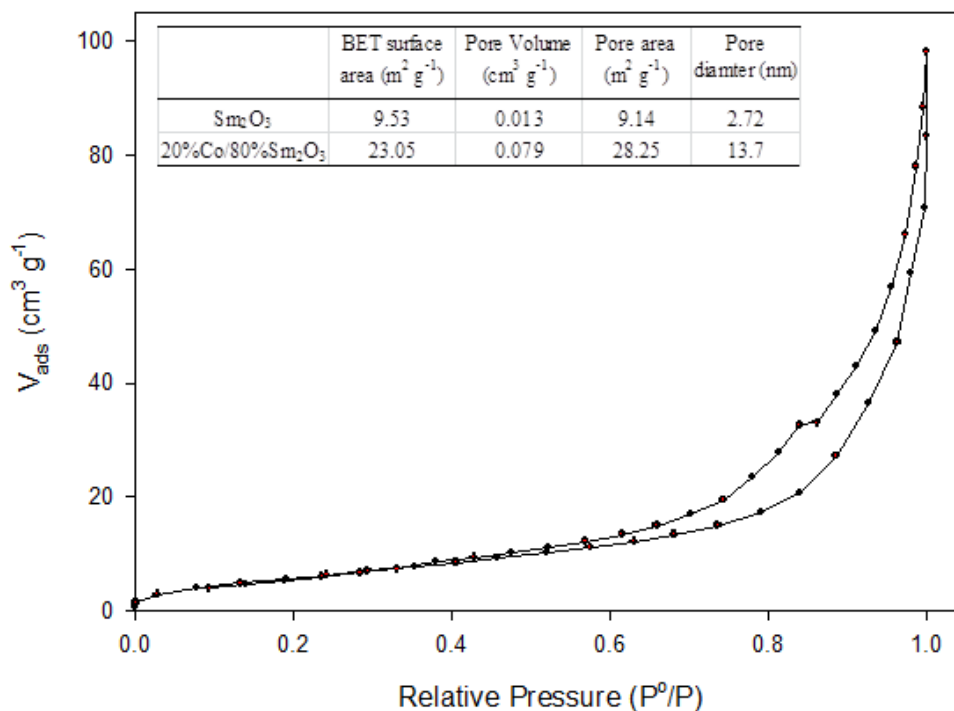

	BET surface area (m^2 g^{-1})	Pore Volume (cm^3 g^{-1})	Pore area (m^2 g^{-1})	Pore diamter (nm)
Sm$_2$O$_3$	9.53	0.013	9.14	2.72
20%Co/80%Sm$_2$O$_3$	23.05	0.079	28.25	13.7

Figure 6: N$_2$ adsorption-desorption isotherm of the 20wt%Co/80wt%Sm$_2$O$_3$ catalyst
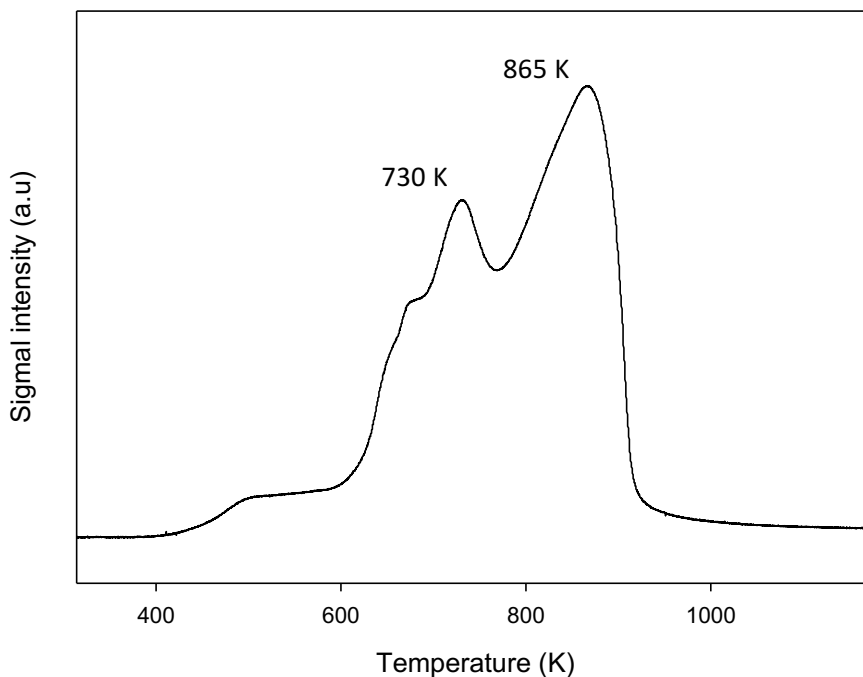
Figure 7: H_2-TPR profile of the $20wt\%Co/80wt\%Sm_2O_3$ catalyst

3.2   Catalytic performance of the 20wt%Co/80wt%Sm₂O₃ catalyst

Figure 8 depicts the catalytic performance of the $20wt\%Co/80wt\%Sm_2O_3$ catalyst in terms of conversion, yield and selectivity. It can be seen that the CH_4 and CO_2 conversions increases with the reaction temperatures (Figure 8a). The CH_4 conversion increases from 16% at 923 K to a maximum value of 70.6% at 1023 K. For CO_2, the conversion increases from 25% at 923 K   and peaked at 72.5%. Typically, the increasing trend of the CH_4 and CO_2 conversion with temperature is consistent with the Arrhenius observation for temperature dependent reactions such as, methane dry reforming [22]. It is noteworthy that the CO_2 conversion is slightly higher than that of CH_4, which could be attributed to the influence of reverse-water-gas-shift reaction. Similar trend has been reported in our previous work using $20wt\%Co/80wt\%CeO_2$ catalyst [15]. Besides, the contributions of reverse water gas shift reaction to the methane dry reforming could also influence the higher conversion of CO_2 compared to CH_4 as reported by Hao et al. [23] for methane dry reforming reaction over $20wt\%Co/80wt\%Al_2O_3$ catalyst. The comparison of the catalytic performance of the $20wt\%Co/80wt\%Sm_2O_3$ catalyst with literature is shown in Table 1. The highest CH_4 and CO_2 conversion of 70.6% and 73.5% obtained in this study is lower than that reported by [24] and [25] for Co/Al_2O_3, Co/MgO and Co/CeO_2 catalysts respectively. The Co/Sm_2O_3 catalyst however displayed higher conversion compared to that reported by [26] and [27] for Co/SiO_2, Co/TiO_2 and Co/CaO catalysts respectively. This could be due to differences in the physicochemical properties of the catalysts, for instance the variation in the BET specific surface area of the reported catalysts as well as the interfacial properties. Figure 8b show that catalytic performance of the $20wt\%Co/80wt\%Sm_2O_3$ catalyst in terms of H_2 and CO yields. The H_2 and CO yields significantly increase with temperature resulting to the highest activity (H_2 yield = 62.29%, CO yield 73.19%) at 1023 K. The increasing trends of the yields with temperature is also typical of Arrhenius-type behaviour for temperature-dependent chemical reaction [22]. Interestingly, CO yield is 11.19% higher than H_2 yield which could be as a result of the contribution of reverse Boudouard reaction [30]. Furthermore, the lower value of H_2 yield obtained compared to CO yield could be due to the influence of reverse water gas shift reaction [31]. The highest values of H_2 and CO yields obtained in this study is lower compare to that of Co/Al_2O_3 and Co/MgO but howerver higher compare to Co/CeO_2 reported by Abasaeed et al. [14]. Furthermore, it is noteworthy, that the methane dry reforming over Co/Sm_2O_3 catalyst produced syngas ratio of ~ 0.9, suitable as feedstock for the production of oxygenated fuel via FTS. Figure 8c depicts the selectivity of the $20wt\%Co/80wt\%Sm_2O_3$ catalyst to H_2 and CO production from the methane dry reforming. Interestingly, both the H_2 and CO selectivity increases with temperature. The H_2 selectivity increases from 11% at 923 K to 82% at 1023 K. Similarly, The CO selectivity increases from 5.8% at 973 K to 61% at 1023 K. Indeed, methane dry reforming over $20wt\%Co/80wt\%Sm_2O_3$ catalyst could be a potential route for Hydrogen production based on the high H_2 selectivity obtained from this study.
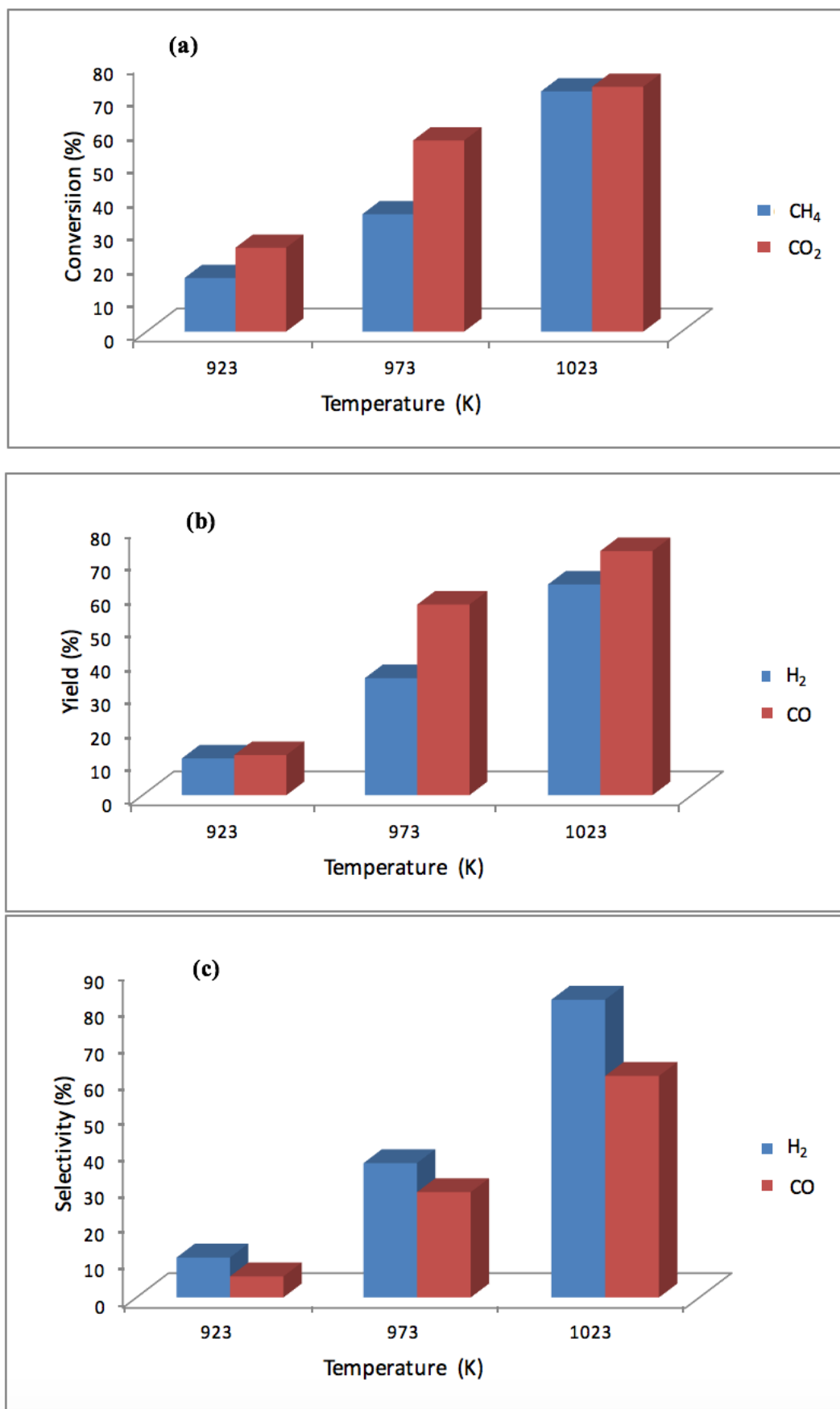
Figure 8: Catalyst performance of the 20wt%Co/80wt%Sm_2O_3 catalyst showing the (a) conversion (b) yield and (c) selectivity ((GHSV = 30000 h^{-1}, P = 1 atm, CH_4:CO_2 =1)

Table 1: Comparison of activity of the Co/Sm$_2$O$_3$ with literature

Catalyst	BET specific surface area (m^2 g^{-1})	CH$_4$ conversion (%)	CO$_2$ conversion (%)	H$_2$ yield (%)	CO yield (%)	Reaction Temp (K)	Reference
Co/Sm$_2$O$_3$	28.25	70.60	73.50	62.25	73.19	1023	This work
Co/Al$_2$O$_3$	53.00	86.50	88.10	84.80	87.30	973	[24]
Co/CeO$_2$	67.00	85.00	92.00	NR	NR	1073	[25]
Co/MgO	22.00	91.90	93.90	89.80	92.90	973	[24]
Co/SiO$_2$	185.00	24.00	36.70	17.90	30.30	873	[26]
Co/TiO$_2$	4.00	20.50	35.30	8.8	28.8	1173	[27]
Co/CaO	5.00	38.60	54.30	31.90	46.30	1173	[24]

NR = Not reported

3.4 *Characterization of the used catalyst for carbon deposition*

Figure 9 shows the amount of carbon deposition per gram 20wt%Co/80wt%Sm$_2$O$_3$ catalyst based on the carbon balance estimated from the methane dry reforming reaction. It is evidence that carbon deposition increases with increase in temperature which is one of the features that characterize methane dry reforming. After about 4 h time-on-stream ,the used 20wt%Co/80wt%Sm$_2$O$_3$ catalyst was characterized for carbon deposition using temperature programmed oxidation (TPO), and SEM-EDX. Figure 10 shows the TPO profile obtained for the spent catalyst using TGA. In order to exclude the interference of moisture in the quantification of the carbon deposition from the TPO, the spent catalysed was analysed excluding weight loss before 373 K. Significantly, it can be visualized from the TPO profile of weight loss that take place at peak temperatures ranged 540-670 K which can be attributed to the oxidation of active (amorphous) carbon. Interestingly, the presence of inert (graphite) carbon which is usually associated with the peak temperature > 773 K cannot be detected. An estimation of the amount of carbon deposited on the spent catalyst show that a total weight loss of 23.18% representing 1.41 mg of the active carbon was oxidized. The evidence of carbon deposition was further ascertained from the morphology of the spent catalyst shown in Figure 11 (a). The SEM micrograph showed clearly the deposition of amorphous carbon on the surface of the catalyst. The amorphous carbon has been reported to have minor effect on the methane dry reforming reaction due to the ease at which it can be gasified by the free valence oxygen provided by the Sm$_2$O$_3$ support [32]. Further analyses of the spent catalyst for elemental composition by EDX micrograph show the presence of elemental carbon (Figure 11 (b)). However, based on the EDX dot mapping in Figure 11 (c), the used catalyst still show the presence of essential components (Co, Sm, and O) which indicate that the catalyst structure was not completely altered by the presence of the amorphous carbon.

4. CONCLUSIONS

In this study, the synthesis, characterization and performance of 20wt%Co/80wt%Sm$_2$O$_3$ catalyst in methane dry reforming for syngas production has been reported. The catalyst was synthesized via wet impregnation and characterized for its physicochemical properties using different techniques. The catalyst performance in the methane dry reforming gave the highest activity at reaction temperature of 1023 K leading to CH$_4$ and CO$_2$ conversions of ~71% and ~73% as well as H$_2$ and CO yields of ~61% and ~73%, respectively. The characterization of the used Co/Sm$_2$O$_3$ by TGA, SEM and EDX confirm the deposition of amorphous carbon which can easily be gasified thereby prolonging the stability of the catalyst with increase TOS. This study has demonstrated the potential of syngas production from methane dry reforming over 20wt%Co/80wt%Sm$_2$O$_3$ catalyst.
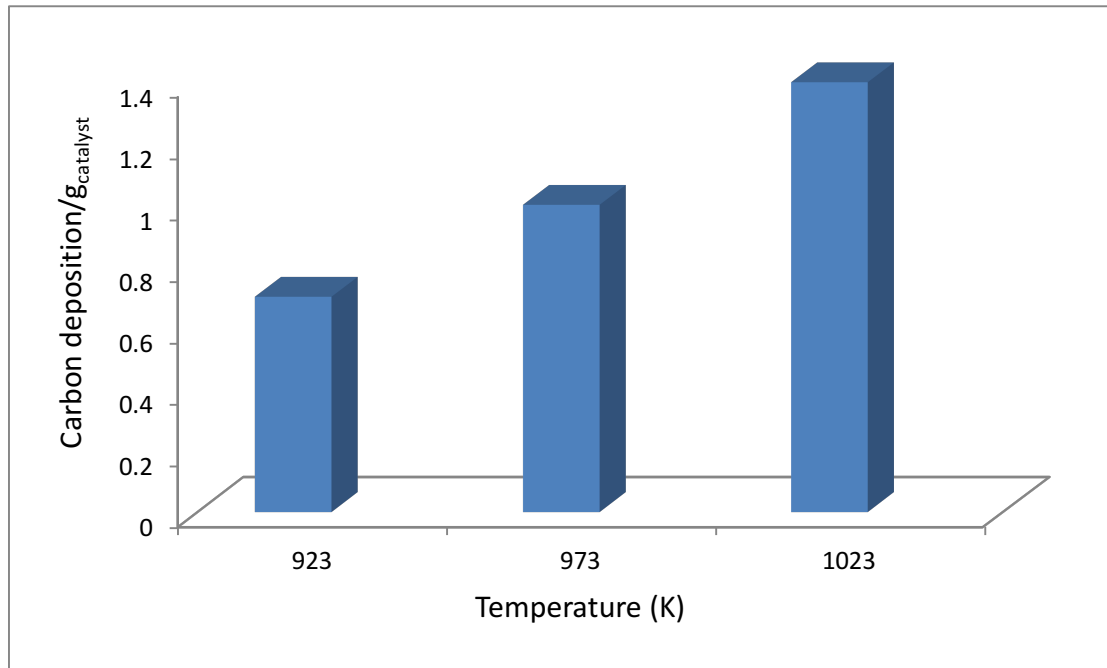
Figure 9: Carbon deposition/g 20wt%Co/80wt%Sm$_2$O$_3$ catalyst (GHSV = 30000 h^{-1}, P = 1 atm, CH$_4$:CO$_2$ =1)
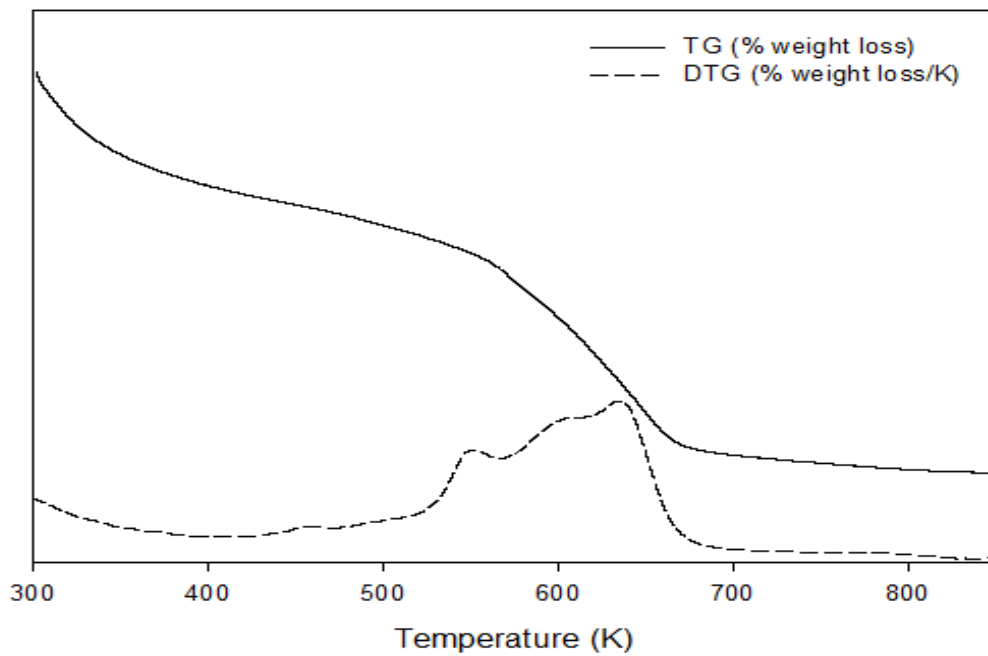

Figure 10: Temperature programmed oxidation of the spent catalyst

Figure 11: EDX micrograph of the spent 20wt%Co/80wt%Sm$_2$O$_3$ catalyst

ACKNOWLEDGEMENTS

REFERENCES

[1]   M.A. Naeem, A.S. Al-Fatesh, W.U. Khan, A.E. Abasaeed, A.H. Fakeeha, Syngas Production from Dry Reforming of Methane over Nano Ni Polyol Catalysts, Int. J. Chem. Eng. Appl. 4 (2013) 315–320. doi:10.7763/IJCEA.2013.V4.317.

[2]   D. Pakhare, J. Spivey, A review of dry (CO$_2$) reforming of methane over noble metal catalysts, Chem. Soc. Rev. 43 (2014) -. doi:10.1039/c3cs60395d.

[3]   K. Aasberg-Petersen, I. Dybkjær, C. V. Ovesen, N.C. Schjødt, J. Sehested, S.G. Thomsen, Natural gas to synthesis gas - Catalysts and catalytic processes, J. Nat. Gas Sci. Eng. 3 (2011) 423–459. doi:10.1016/j.jngse.2011.03.004.

[4]   J.R.H. Ross, Natural gas reforming and CO$_2$ mitigation, Catal. Today. 100 (2005) 151–158. doi:10.1016/j.cattod.2005.03.044.

[5]   A. Braga, T. P., Santos, R. C., Sales, B. M., da Silva, B. R., Pinheiro, A. N., Leite, E. R., & Valentini, CO2 mitigation by carbon nanotube formation during dry reforming of methane analyzed by factorial design combined with response surface methodology, Chinese J. Catal. 35 (2014) 514–523. doi:10.1016/S1872-2067(14)60018-8.

[6]   G.S. Gallego, C. Batiot-Dupeyrat, J. Barrault, E. Florez, F. Mondragón, Dry reforming of methane over LaNi1−yByO3±δ (B=Mg, Co) perovskites used as catalyst precursor, Appl. Catal. A Gen. 334 (2008) 251–258. doi:10.1016/j.apcata.2007.10.010.

[7]   P. Forzatti, L. Lietti, Catalyst deactivation, 52 (1999) 165–181.

[8]   H. He, J.M. Hill, Carbon deposition on Ni/YSZ composites exposed to humidified methane, Appl. Catal. A Gen. 317 (2007) 284–292. doi:10.1016/j.apcata.2006.10.040.

[9]   X.E. Verykios, Catalytic dry reforming of natural gas for the production of chemicals and hydrogen, Int. J. Hydrogen Energy. 28 (2003) 1045–1063. doi:10.1016/S0360-3199(02)00215-X.

[10]   G. Sierra Gallego, F. Mondragón, J.-M. Tatibouët, J. Barrault, C. Batiot-Dupeyrat, Carbon dioxide reforming of

methane over La_2NiO_4 as catalyst precursor—Characterization of carbon deposition, Catal. Today. 133-135 (2008) 200–209. doi:10.1016/j.cattod.2007.12.075.

[11]   J. Zhang, H. Wang, A.K. Dalai, Kinetic Studies of Carbon Dioxide Reforming of Methane over Ni−Co/Al−Mg−O Bimetallic Catalyst, Ind. Eng. Chem. Res. 48 (2009) 677–684. doi:10.1021/ie801078p.

[12]   D. Pakhare, J. Spivey, A review of dry (CO_2) reforming of methane over noble metal catalysts, Chem. Soc. Rev. 43 (2014) -. doi:10.1039/c3cs60395d.

[13]   J. Sehested, Four challenges for nickel steam-reforming catalysts, Catal. Today. 111 (2006) 103–110. doi:10.1016/j.cattod.2005.10.002.

[14]   A.E. Abasaeed, A.S. Al-fatesh, M.A. Naeem, A.A. Ibrahim, A.H. Fakeeha, Catalytic performance of CeO_2 and ZrO_2 supported Co catalysts for hydrogen production via dry reforming of methane, Int. Hydrog. Energy. (2015) 6818–6826. doi:http://dx.doi.org/10.1016/j.ijhydene.2015.03.152.

[15]   B. V. Ayodele, M.R. Khan, C.K. Cheng, Catalytic performance of ceria-supported cobalt catalyst for CO-rich hydrogen production from dry reforming of methane, Int. J. Hydrogen Energy. (2015). doi:10.1016/j.ijhydene.2015.10.049.

[16]   A.I. Paksoy, B.S. Caglayan, A.E. Aksoylu, A study on characterization and methane dry reforming performance of Co–Ce/ZrO2 catalyst, Appl. Catal. B Environ. 168-169 (2015) 164–174. doi:10.1016/j.apcatb.2014.12.038.

[17]   S. Sato, R. Takahashi, M. Kobune, H. Gotoh, Basic properties of rare earth oxides, Appl. Catal. A Gen. 356 (2009) 57–63. doi:10.1016/j.apcata.2008.12.019.

[18]   R. Mohammadinasab, M. Tabatabaee, H. Aghaie, M.A. Seyed Sadjadi, A Simple Method for Synthesis of Nanocrystalline Sm2O3 Powder by Thermal Decomposition of Samarium Nitrate, Synth. React. Inorganic, Met. Nano-Metal Chem. 45 (2014) 451–454. doi:10.1080/15533174.2013.819912.

[19]   S. Brunauer, P.H. Emmett, E. Teller, Adsorption of Gases in Multimolecular Layers, J. Am. Chem. Soc. 60 (1938) 309–319. doi:citeulike-article-id:4074706\rdoi: 10.1021/ja01269a023.

[20]   E.P. Barrett, L.G. Joyner, P.P. Halenda, The Determination of Pore Volume and Area Distributions in Porous Substances. I. Computations from Nitrogen Isotherms, J. Am. Chem. Soc. 73 (1951) 373–380. doi:10.1021/ja01145a126.

[21]   C. Ehrhardt, M. Gjikaj, W. Brockner, Thermal decomposition of cobalt nitrato compounds: Preparation of anhydrous cobalt(II)nitrate and its characterisation by Infrared and Raman spectra, Thermochim. Acta. 432 (2005) 36–40. doi:10.1016/j.tca.2005.04.010.

[22]   T.C. Clark, J.E. Dove, Examination of Possible Non-Arrhenius Behavior in the reactions, Can. J. Chem. 51 (1973) 2147–2154. doi:10.1139/v73-323.

[23]   Z. Hao, Q. Zhu, Z. Jiang, H. Li, Fluidization characteristics of aerogel Co/Al_2O_3 catalyst in a magnetic fluidized bed and its application to CH4–CO2 reforming, Powder Technol. 183 (2008) 46–52. doi:10.1016/j.powtec.2007.11.015.

[24]   E. Ruckenstein, H.. Wang, Carbon dioxide reforming of methane to synthesis gas over supported cobalt catalysts, Appl. Catal. A Gen. 204 (2000) 257–263. doi:10.1016/S0926-860X(00)00674-8.

[25]   I. Luisetto, S. Tuti, E. Di Bartolomeo, Co and Ni supported on CeO_2 as selective bimetallic catalyst for dry reforming of methane, Int. J. Hydrogen Energy. 37 (2012) 15992–15999. doi:10.1016/j.ijhydene.2012.08.006.

[26]   R. Bouarab, O. Akdim, A. Auroux, O. Cherifi, C. Mirodatos, Effect of MgO additive on catalytic properties of Co/SiO_2 in the dry reforming of methane, Appl. Catal. A Gen. 264 (2004) 161–168. doi:10.1016/j.apcata.2003.12.039.

[27]   K. Nagaoka, Influence of the reduction temperature on catalytic activity of Co/TiO2 (anatase-type) for high pressure dry reforming of methane, Appl. Catal. A Gen. 255 (2003) 13–21. doi:10.1016/S0926-860X(03)00631-8.

[28]   N. Wang, W. Chu, L. Huang, T. Zhang, Effects of Ce/Zr ratio on the structure and performances of Co-$Ce_{1-x}Zr_xO_2$ catalysts for carbon dioxide reforming of methane, J. Nat. Gas Chem. 19 (2010) 117–122. doi:10.1016/S1003-9953(09)60055-4.

[29] S.M. Sajjadi, M. Haghighi, F. Rahmani, Dry reforming of greenhouse gases CH_4/CO_2 over MgO-promoted Ni-Co/Al_2O_3-ZrO_2 nanocatalyst: effect of MgO addition via sol-gel method on catalytic properties and hydrogen yield, J. Sol-Gel Sci. Technol. (2014) 1–14. doi:10.1007/s10971-014-3280-1.

[30] N. Laosiripojana, W. Sutthisripok, S. Assabumrungrat, Synthesis gas production from dry reforming of methane over CeO_2 doped Ni/Al_2O_3: Influence of the doping ceria on the resistance toward carbon formation, Chem. Eng. J. 112 (2005) 13–22. doi:10.1016/j.cej.2005.06.003.

[31] P. Djinović, J. Batista, A. Pintar, Efficient catalytic abatement of greenhouse gases: Methane reforming with CO_2 using a novel and thermally stable Rh-CeO_2 catalyst, Int. J. Hydrogen Energy. 37 (2012) 2699–2707. doi:10.1016/j.ijhydene.2011.10.107.

[32] X. Tu, J.C. Whitehead, Plasma dry reforming of methane in an atmospheric pressure AC gliding arc discharge: Co-generation of syngas and carbon nanomaterials, Int. J. Hydrogen Energy. 39 (2014) 9658–9669. doi:10.1016/j.ijhydene.2014.04.073.